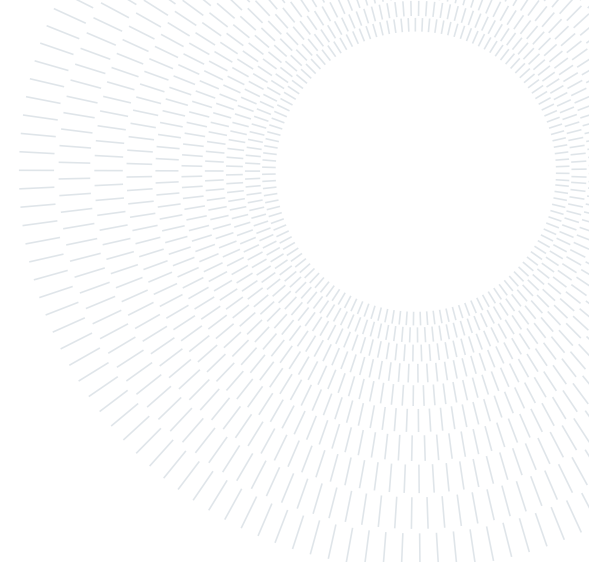




POLITECNICO
MILANO 1863

**SCUOLA DI INGEGNERIA INDUSTRIALE
E DELL'INFORMAZIONE**



EXECUTIVE SUMMARY OF THE THESIS

Control of an Over-Actuated Vehicle for Autonomous Driving and Energy Optimization

LAUREA MAGISTRALE IN AUTOMATION AND CONTROL ENGINEERING - INGEGNERIA DELL'AUTOMAZIONE

Author: GIANMARCO GRANDI

Advisor: PROF. LUCA BASCETTA

Co-advisor: PROF. MIKAEL NYBACKA

Academic year: 2021-2022

1. Introduction

An over-actuated (OA) vehicle is a system that presents more control variables than degrees of freedom. Therefore, more than one configuration of the control input can drive the system to a desired state in the state space, and this redundancy can be exploited to fulfill other tasks and solve additional problems. Nowadays, the energy problem is getting extremely critical and research in this field of study is paramount. Concerning this problem, Over-Actuation offers the possibility to drive the vehicle to the desired state and exploit the redundancy of the control action to choose the one that minimizes energy consumption.

Over-actuation research at KTH has been ongoing for some years, with the goal of exploiting control action redundancy for various purposes. Different over-actuated prototype vehicles have been built with the intention to have an experimental evaluation of the solutions.

In this project, a control strategy is developed to guarantee trajectory following and stability while minimizing the energy consumption of an over-actuated vehicle with four driving wheels and four steering wheels (4WD, 4WS). The con-

troller must be implemented and embedded on the Research Concept Vehicle (RCV-E) (Figure 1) to ensure real-time performance.



Figure 1: RCV-E developed at the Integrated Transport Research Lab (ITRL) within KTH Royal Institute of Technology.

Previous studies developed at KTH explored the energy-efficient control methods and models for an over-actuated vehicle. In P. Sun's work [1, 2], an analysis of front steering wheels (FWS) and torque vectoring (4WD) to directly control the yaw moment (DYC) for stability and energy efficiency purposes is carried out. The

result of an offline optimal torque distribution to minimize the power consumption is exploited to relate the engine efficiency with the yaw moment (Mz) at steady-state cornering.

In J. Edrén's work, importance is also given to energy optimization in [3], where it was noticed that the largest contribution to the reduction of energy consumption during cornering is provided by rear-axle steering: compared to traditional road car driving, the improvements are about 10%.

Further works on over-actuation intending to reduce energy consumption are outlined here. As in [4], the control allocation scheme allocates torque and steering angles to track the vehicle's planar velocities (vx, vy, yaw rate) provided by the upper-level controller. Two cost functions are optimized simultaneously; one for reference tracking and one for the engine's energy minimization. In [5], an OA vehicle with in-wheel electric motors exploits a control strategy to allocate the total reference torque on the two axles. Results show that for straight driving at a constant speed, two-wheel drive is more efficient than four-wheel drive. In [6], an online control system is proposed in order to improve the vehicle's energy efficiency by minimizing tire power losses: tire slip resistance, and rolling losses. In [7], a two-step algorithm is presented to combine vehicle stability and energy minimization. The first step allocates the torques to satisfy the longitudinal force request on the wheels using the in-wheel engine characteristic to minimize power consumption. The second allocation step starts from this result to find a close solution that bounds the longitudinal slip ratio within linear boundaries and provides the requested total traction force. Lateral forces are also considered [8] and estimated to limit the longitudinal ones at the wheels by defining a stability region within the friction circle.

2. Trajectory following

The controller used in this project to track the given trajectory is an MPC, and it must be able to follow the path at the reference speed. Lateral dynamics of the vehicle are controlled by minimizing the lateral deviation from the reference path, whereas tracking the reference velocity controls the longitudinal dynamics. Given

the i -th position of the car along the prediction horizon (x_c^i, y_c^i) and the pose of the i -th reference point $(x_r^i, y_r^i, \theta_r^i)$, the lateral deviation is computed as follows:

$$LD = -x_c^i \sin \theta_r^i + y_c^i \cos \theta_r^i + x_r^i \sin \theta_r^i - y_r^i \cos \theta_r^i \quad (1)$$

Since the objective of the controller is to have $LD = 0$, Equation 1 can be written as a function of the vehicle state as follows:

$$[-\sin \theta_r^i, \cos \theta_r^i] \begin{bmatrix} x_c^i \\ y_c^i \end{bmatrix} = -x_r^i \sin \theta_r^i + y_r^i \cos \theta_r^i \quad (2)$$

Besides, since the Over-Actuation allows to control rotation and lateral motion independently from each other, the desired vehicle direction θ_r can be arbitrarily provided as an additional reference to track. One advantage of having this DoF tunable by a path planner is that it is possible to force lateral motion, with the vehicle yaw angle fixed, to improve vehicle stability as in a double-lane change. From Equation 2, the output of the system and the reference to track can be rewritten as:

$$y^i = C^i x^i$$

$$r^i = \begin{bmatrix} -x_r^i \sin \theta_r^i + y_r^i \cos \theta_r^i \\ \theta_r^i \\ v_{xr}^i \end{bmatrix} \quad (3)$$

with

$$C^i = \begin{bmatrix} -\sin \theta_r^i & \cos \theta_r^i & 0 & 0 & 0 & 0 \\ 0 & 0 & 1 & 0 & 0 & 0 \\ 0 & 0 & 0 & 1 & 0 & 0 \end{bmatrix}$$

where x^i is the vehicle state computed at the i -th step over the prediction horizon defined as follows.

$$x = [x_{car}, y_{car}, \theta, v_x, v_y, \dot{\theta}]^T \quad (4)$$

3. Sources of energy consumption

Different sources of energy loss in electric vehicles are investigated in this research; despite this, only those that over-actuation (4WD, 4WS) can directly influence are considered. In particular, three sources of energy loss are identified.

First are the losses due to longitudinal slip P_σ , where the traction force due to tire slip is opposed to the sliding velocity of the contact patch and dissipates power. These are defined in [6] as follows.

$$P_\sigma = -F_x v_s \quad (5)$$

where $v_s = r\omega - v_x = \sigma_x r\omega$

and F_x is the longitudinal force at the contact patch, v_x is the wheel's longitudinal velocity, r is the wheel's radius, ω is the wheel's rotational velocity, and σ_x is the longitudinal slip ratio.

From Equation 5, P_σ becomes

$$P_\sigma = -F_x \sigma_x r\omega = -C_\sigma F_z r\omega \sigma_x^2 \quad (6)$$

$$\text{with } F_x = C_\sigma F_z \sigma_x$$

and C_σ is the normalized longitudinal slip stiffness.

Second, losses due to cornering resistance P_y , as

$$P_y = F_y v_y = -C_\alpha F_z v_x \alpha^2 \quad (7)$$

with $F_y = -C_\alpha F_z \alpha$
and $v_y = v_x \alpha$

where F_y is the cornering resistance, v_y is the lateral velocity of the wheel, C_α is the cornering stiffness, α is the sideslip angle or slip angle, and v_x is the longitudinal velocity of the wheel.

Third, losses in the motor $P_{engineLoss}$ due to power conversion and dependent on the engine efficiency characteristic.

$$P_{engineLoss} = P_{El} - P_{Mech} = \frac{T\omega}{\eta} \quad (8)$$

where P_{El} is the Electrical Power provided to the engine, P_{Mech} is the Mechanical Power provided at the shaft, and η is the efficiency of the engine, which is dependent to the operating conditions (T, ω) .

4. Trajectory-following control strategy

The controller solves the allocation problem by allocating eight control variables:

$$u = [T_{fl}, T_{fr}, T_{rr}, T_{rl}, \delta_{fl}, \delta_{fr}, \delta_{rr}, \delta_{rl}]^T \quad (9)$$

where T_i is the torque at the wheels and δ_i is the wheel's steering angles.

For this purpose, a structured control strategy is suggested here. A two-level control structure is needed to separately control low-frequency dynamics for the trajectory-following task and high-frequency dynamics for generating the control action (Eq. 9) at the wheels. In this regard, the upper-level controller (LTV-MPC) is responsible for allocating the forces at the wheels in the vehicle reference frame (FX_i, FY_i) , as shown in Figure 2a, whereas the lower-level controller transforms these forces in the wheel's reference frame, as in Figure 2b, and derives torque and steering angle using Equation 11.

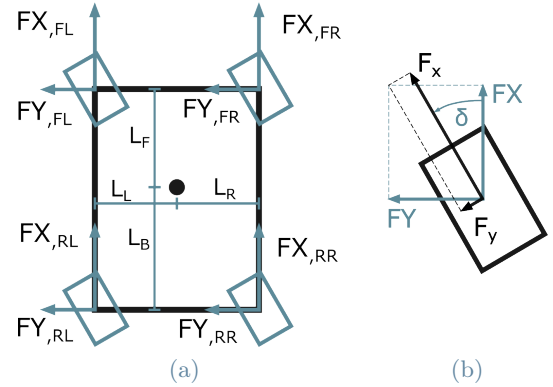


Figure 2: Two-level model. a) Is the model utilized by the LTV-MPC. b) Is the model utilized by the lower level controller to allocate the forces for each wheel.

The equations of the model used for the upper-level controller are as follows.

$$\begin{aligned} \dot{x}_{car} &= v_x \cos \theta - v_y \sin \theta \\ \dot{y}_{car} &= v_x \sin \theta + v_y \cos \theta \\ \dot{\theta} &= \dot{\theta} \\ \dot{v}_x &= v_y \dot{\theta} + \frac{F_x}{m} \\ \dot{v}_y &= -v_x \dot{\theta} + \frac{F_y}{m} \\ \ddot{\theta} &= \frac{M_z}{J} \end{aligned} \quad (10)$$

with

$$\begin{aligned} F_x &= F_{X_{fl}} + F_{X_{fr}} + F_{X_{rr}} + F_{X_{rl}} \\ F_y &= F_{Y_{fl}} + F_{Y_{fr}} + F_{Y_{rr}} + F_{Y_{rl}} \\ M_z &= -(F_{X_{fl}} + F_{X_{rl}}) * l_l + (F_{X_{fr}} + F_{X_{rr}}) * l_r + (F_{Y_{fl}} + F_{Y_{fr}}) * l_f - (F_{Y_{rr}} + F_{Y_{rl}}) * l_b \end{aligned}$$

Whereas the equations of the model for the lower-level controller are:

$$\begin{aligned} F_{x,i} &= FX_i \cos(\delta_i) + FY_i \sin(\delta_i) \\ F_{y,i} &= -FX_i \sin(\delta_i) + FY_i \cos(\delta_i) \\ T_i &= F_{x,i} * r_w \\ \delta_i &= \frac{F_{y,i}}{C_\alpha * F_{z_i}} + \alpha_i \quad i = fl, fr, rr, rl \end{aligned} \quad (11)$$

The LTV-MPC can be formulated as a quadratic problem, as follows.

$$\begin{aligned} \min_{U(k)} & [R(k) - Y(k)]^T Q_0 [R(k) - Y(k)] + \\ & + U^T(k) R_0 U(k) \\ \text{s.t.} & \quad x(k+i+1) = A_{k+i} x(k+i) + \\ & \quad + B_{k+i} u(k+i) + G_{k+i} \\ & \quad y(k+i) = C_{k+i} x(k+i) \\ & \quad LB \leq V \cdot U(k) \leq UB \\ & \quad \forall i = 0, \dots, N-1 \end{aligned} \quad (12)$$

where Q_0 and R_0 are the positive definite weight matrices, V is a matrix for the constraints definition, and LB and UB are the lower and upper bounds of the constraints.

A simple open-loop solver is used to control the lower-level system.

The division adopted to structure the vehicle's controller allows for considering stability conditions at the wheels directly in the LTV-MPC. The friction circle constraint limits the forces at the wheels (FX_i, FY_i) and keeps them in the stable region. However, it is a nonlinear constraint, and to include it in the LTV-MPC formulation, the friction circle is approximated to an octagon, such that the sides of the polygon can be expressed as linear constraints in the cost function (Eq. 12). Besides, an integral action is added in the LTV-MPC to improve the longitudinal speed tracking.

4.1. Results

The results obtained in the simulation to evaluate the controller performance in tracking the reference trajectory are shown in Table 1. Here, three maneuvers are investigated. 1) Driving on a mixed-profile road with corners and straight lines, 2) on a straight line, including acceleration, steady-state driving (130 km/h), and

braking, with a double lane change maneuver to mimic an overpass, where the reference yaw angle points in the same direction, and 3) steady-state cornering on a 30m-radius turn at 50 km/h. Tests are performed for six combinations of the prediction horizon:

- 1) A prediction horizon (Th) of 2.0 s with a sampling time (Ts) of 0.2 s and 10 samples (N).
- 2) Th = 1.5 s, Ts = 0.15 s and N=10.
- 3) Th = 1.0 s, Ts = 0.1 s and N=10.
- 4) Th = 1.4 s, Ts = 0.2 s and N=7.
- 5) Th = 1.5 s, Ts = 0.3 s and N=5.
- 6) Th = 1.0 s, Ts = 0.2 s and N=5.

Mixed-profile Road		
MPC comb.	LD RMSE	YAW RMSE
1)	0.193	0.024
2)	0.171	0.019
3)	0.124	0.014
4)	0.217	0.022
5)	0.307	0.034
6)	0.176	0.021
Straight Road		
MPC comb.	LD RMSE	YAW RMSE
1)	0.087	0.006
2)	0.076	0.010
3)	0.078	0.053
4)	0.086	0.019
5)	0.110	0.027
6)	0.075	0.050
Steady-state cornering		
MPC comb.	LD RMSE	YAW RMSE
1)	0.347	0.007
2)	0.268	0.005
3)	0.176	0.004
4)	0.382	0.010
5)	0.561	0.016
6)	0.279	0.014

Table 1: Results of the controller for trajectory following performance during the three maneuvers. The RMSE of the lateral deviation from the reference path and the RMSE of the yaw angle tracking are reported.

From Table 1, it is possible to notice that lateral deviation mostly depends on the sampling time of the MPC. When the samples are closer to one another, the vehicle tends to cut less of the path, and the lateral deviation is smaller.

The prediction horizon has some impact as well, though less. When the MPC's vision field is shorter, it tries to stick as close as possible to the path just ahead of it, disregarding points farther away; therefore, it does not jeopardize the tracking of the near points for the remote ones.

Regarding yaw angle tracking, the same behavior affects the result. The more the vehicle cuts corners, the less tangent its direction will be to the trajectory.

Concerning velocity tracking, all the configuration can track the desired velocity at the limits of the vehicle thrust and the error at steady-state conditions is null.

5. Energy Minimization

To minimize the energy consumed by the vehicle, control techniques must exploit the over-actuation to influence the sources of energy loss investigated in Section 3. For this purpose, two solutions are investigated to act on wheel losses and engine efficiency.

In Equations 6 and 7, quadratic relations between power losses at the wheels and the longitudinal and lateral slips are derived. To minimize power losses, the slips (longitudinal and lateral) must be equal for all four wheels. To create this condition, the requested forces (FX_i , FY_i) at the wheels (Figure 2a) must be proportional to the normal ones ($F_{z,i}$). To achieve this result, the weighting term R_0 of the quadratic cost function (Eq. 12) should have its terms inversely proportional to the normal forces ($F_{z,i}$) on the wheels, so that the higher is the normal force on one wheel the lower the control action is penalized.

In addition, this solution, allocating the forces proportionally to $F_{z,i}$, allows for exploiting better tire availability maximizing the distance of the wheel's forces (FX_i , FY_i) to the friction circle limit. The result is less wheel saturation and higher wheel stability.

The results on energy reduction are reported in Section 5.1.

Concerning the power losses due to the engine efficiency, the ideal solution is to model and include them inside the LTV-MPC cost function. In this way, the LTV-MPC solution minimizes the energy consumed along the horizon. How-

ever, the nonlinear efficiency characteristic of the engines must be linearized to be included in the cost function, with consequent loss of information. The LTV-MPC's solution does not find convenient points of the engine characteristic but reduces the energy lost along the prediction horizon by minimizing the torques and the speeds of all the engines. The consequence is a reduction in the vehicle velocity and a worse pursuit of the reference.

An additional allocation step is used to incorporate the engine's nonlinear efficiency characteristic into the controller. This step redistributes the FX forces provided by the LTV-MPC between the front and rear axles of the vehicle based on the nonlinear efficiency characteristic. The two sides are independent to preserve the yaw moment provided by the longitudinal forces, and the friction circle constraint is still satisfied. Results on this solution in terms of energy minimization are reported in section 5.1.

5.1. Results

The tests are performed to compare the cases when no energy minimization strategy is implemented (B), when only the vehicle's weight distribution on the wheels is considered (W), and when, in addition to weight distribution, also the engine efficiency optimization strategy is included (E).

Three maneuvers are investigated. 1) Straight acceleration of $2m/s^2$ on average, 2) Straight acceleration of $8.5m/s^2$ on average, 3) Steady-state cornering at $50km/h$ on a 30m-radius turn. At the end of these maneuvers, five power source measurements were obtained.

1. The electric power requested by the engines.
2. The power lost in the motors, computed using the engine efficiency characteristic.
3. The mechanical power at the shaft of the four engines.
4. The power lost due to wheel slipping, computed according to Equation 6, only for positive longitudinal forces at the wheels F_x since braking is not considered.
5. The power lost due to wheel cornering, computed according to Equation 7.

For each of the five terms, the energy was computed as the time integral of the power during the maneuvers.

Results are shown in Table 2.

Weight distribution affects losses at the wheels more when the sideslip angles and slip ratio are higher, so during cornering and severe accelerations. Results show that during high acceleration the reduction of the energy wasted due to longitudinal slip reaches 11%; nevertheless, the torque distribution, proportional to the wheel's vertical forces, is not optimized for the energy wasted in the engines, which results in a null advantage in the electric energy consumed. During steady-state cornering, the reduction of the energy wasted due to lateral sliding is 29% for the case investigated, and since the engine torque is less affected, this reduction impacts more on the electric energy provided to the engines, which decreases only to 19%.

Concerning engine energy loss reduction, results show that when the total requested torque is sufficiently low, the reallocation step is better exploited, and the overall torque is delivered only by the rear wheels that work at more efficient engine conditions. In this regard, this technique affects more low accelerations and steady-state cornering, reducing the overall electric energy by 2% during straight acceleration and by 13% during steady-state cornering. However, this solution increases the longitudinal slip losses.

6. Implementation of the controller on the RCV-E

MicroAutoBox II - dSPACE is used as control interface to manage sensors, actuators and software of the RCV-E. To integrate the controller into the dSPACE platform, the DAQP solver [9] is adopted to solve the quadratic problem of the LTV-MPC.

The real-time performance is affected only by the prediction horizon (N) chosen for the LTV-MPC. Therefore, multiple prediction horizons have been tested to assess the limits of the solution.

Results in Table 3 show that the controller does not suffer from execution problems in real-time. In particular, the control sample time used in the simulations for the LTV-MPC is 0.1 s, which would limit the prediction horizon of the controller to 12 samples. This value is sufficiently high to guarantee excellent performance of trajectory following and energy minimization.

2 m/s ² average acceleration					
Case	Elect. En	Eng. Loss	Mech. En	Slip loss	Cor. Res.
B	1075.4	163.7	911.7	12.03	0.00
W	1075.1	163.5	911.6	11.91	0.00
E	1052.6	126.0	926.6	28.29	0.00
8.5 m/s ² average acceleration					
Case	Elect. En	Eng. Loss	Mech. En	Slip loss	Cor. Res.
B	1029.6	116.2	913.4	36.28	0.01
W	1028.8	118.5	910.3	32.27	0.01
E	1028.7	115.9	912.8	35.14	0.01
Steady-state cornering					
Case	Elect. En	Eng. Loss	Mech. En	Slip loss	Cor. Res.
B	197.5	72.9	124.6	0.70	79.28
W	154.0	55.5	98.6	0.16	54.90
E	134.7	35.3	99.4	0.45	55.60

Table 2: Energy consumed by the LTV-MPC with parameters (Th=1.5 s, Ts=0.15 s, N=10) during the different Maneuvers. All the values are expressed in kilo-Joule (kJ).

Prediction Horizon N	Execution time
N = 5	0.005 s
N = 7	0.014 s
N = 10	0.033 s
N = 12	0.086 s
N = 13	0.113 s
N = 15	0.129 s

Table 3: Execution time of the controller on dSPACE - MicroAutoBox II.

7. Conclusion

From the results illustrated in Sections 4.1 and 5.1, the vehicle can follow the provided trajectory for all the combinations of prediction horizons investigated, and the two control techniques investigated can successfully exploit over-actuation to reduce energy consumption. In particular, the highest improvements are obtained during cornering, where the two techniques sum their effects up, whereas, for the longitudinal case, slip reduction and engine loss minimization have conflicting effects. Last, the controller

did not show issues in the embedded real-time performance. As a result, a critical vision of the developed control strategy may suggest that a more computationally expensive solution can be exploited to achieve further improvements while staying within the margins observed from real-time performance.

References

- [1] Peikun Sun, Annika Trigell, Lars Drugge, and Jenny Jerrelind. Energy efficiency and stability of electric vehicles utilising direct yaw moment control. *Vehicle System Dynamics*, 60:1–21, 11 2020.
- [2] Peikun Sun, Annika Stensson Trigell, Lars Drugge, and Jenny Jerrelind. Energy-efficient direct yaw moment control for in-wheel motor electric vehicles utilising motor efficiency maps. *Energies*, 13(3), 2020.
- [3] Johannes Edrén, Mats Jonasson, Jenny Jerrelind, Annika Stensson Trigell, and Lars Drugge. Energy efficient cornering using over-actuation. *Mechatronics*, 59:69–81, 2019.
- [4] Jonathan Brembeck and Peter Ritzer. Energy optimal control of an over actuated robotic electric vehicle using enhanced control allocation approaches. In *2012 IEEE Intelligent Vehicles Symposium*, pages 322–327, 2012.
- [5] Xinwei Jiang, Long Chen, Xing Xu, Yingfeng Cai, Yong Li, and Wujie Wang. Analysis and optimization of energy efficiency for an electric vehicle with four independent drive in-wheel motors. *Advances in Mechanical Engineering*, 10:168781401876554, 03 2018.
- [6] Naser Sina, Mohammad Reza Hairi Yazdi, and Vahid Esfahanian. A novel method to improve vehicle energy efficiency: Minimization of tire power loss. *Proceedings of the Institution of Mechanical Engineers, Part D: Journal of Automobile Engineering*, 234(4):1153–1166, 2020.
- [7] Houhua Jing, Fengjiao Jia, Haifeng Liu, and Jiapeng Sun. Multi-objective optimal control allocation for a four-wheel-independent-drive electric vehicle. In *2017 36th Chinese Control Conference (CCC)*, pages 9543–9547, 2017.
- [8] T. Bächle, K. Graichen, M. Buchholz, and K. Dietmayer. Model predictive control allocation in electric vehicle drive trains. *IFAC-PapersOnLine*, 48(15):335–340, 2015. 4th IFAC Workshop on Engine and Powertrain Control, Simulation and Modeling E-COSM 2015.
- [9] Daniel Arnström. DAQP software. <https://github.com/darnstrom/daqp>.